

Semicrystalline block copolymers in rigid confining nanopores

Man Yan Eric Yau,[†] Ilja Gunkel,^{‡,¶} Brigitte Hartmann-Azanza,[†] Wajiha Akram,[†] Yong Wang,[§] Thomas Thurn-Albrecht,^{‡,¶} Martin Steinhart^{†,*}

[†]Institut für Chemie neuer Materialien, Universität Osnabrück, Barbarastr.7, 49076 Osnabrück, Germany

[‡]Martin-Luther-Universität Halle-Wittenberg, Institut für Physik, D-06099 Halle, Germany

[¶]Current address: Adolphe Merkle Institute, Chemin des Verdiers 4, 1700 Fribourg, Switzerland

[§]Nanjing Tech University, State Key Lab of Materials-Oriented Chemical Engineering; College of Chemical Engineering, Xin Mofan Road 5, Nanjing 210009, Jiangsu, China

E-mail: thomas.thurn-albrecht@physik.uni-halle.de; martin.steinhart@uos.de

Supporting text 1:

Bulk behaviour of the symmetric PS-*b*-PLLA used in this work – thermal analysis

The DSC heating scans of bulk symmetric PS-*b*-PLLA displayed in Figure S1 were measured with a Perkin Elmer Diamond DSC. The samples were heated from 30°C up to 180°C at a rate of 10 K/min (1st heating scan) and kept at 180°C (PLLA is molten) for 10 min to erase the thermal history. Subsequently, the PS-*b*-PLLA was cooled to 30°C (below the glass transition temperature of PLLA) at rates of -160 K/min (quenching), -10 K/min and -1 K/min (1st cooling scan). Finally, the samples were heated to 180°C at a rate of 10 K/min (2nd heating scan). During the second heating runs, exothermic cold crystallization peaks having their minima at $T_C = 124^\circ\text{C}$ were observed for cooling rates of -160 K/min and -10 K/min, but after cooling at -1 K/min no crystallization exotherm appeared. The areas of the exothermic PLLA crystallization peaks appearing in the second heating runs correspond to the enthalpies ΔH_C of the underlying cold crystallization processes. Independent of the applied cooling rate all second heating runs showed pronounced endothermic melting peaks with maxima at $T_M = 173^\circ\text{C}$. The areas of the endothermic PLLA melting peaks correspond to the PLLA melting enthalpies ΔH_M . The ratio $\Delta H_C/\Delta H_M$ reveals the relative proportion of crystalline PLLA that was not crystallized in the course of the first cooling run preceding the second heating run. All crystalline PLLA melting during the second heating run had already crystallized during the first cooling for a cooling rate of -1 K/min, as no endothermic crystallization peak was apparent in the second heating run ($\Delta H_C/\Delta H_M = 0$). Cooling at -10 K/min yielded $\Delta H_C/\Delta H_M = 0.8$, indicating that only 20% of the PLLA that melted in the second heating run had crystallized during the first cooling run. Quenching PS-*b*-PLLA at -160 K/min yielded $\Delta H_C/\Delta H_M = 1.0$. This outcome suggests that quenching PS-*b*-PLLA at -160 K/min completely prevents crystallization of the PLLA blocks.

The DSC cooling scans of bulk PS-*b*-PLLA shown in Figure S2 of the Supporting Information were obtained using a Perkin Elmer DSC 8500. The PS-*b*-PLLA was kept at 190°C for 10 minutes to erase the thermal history and then cooled at the specified cooling rates. At a cooling rate of -10 K/min the minimum of the crystallization endotherm occurred at $T_C \sim 99^\circ\text{C}$; at a cooling rate of -1 K/min the minimum of the crystallization endotherm occurred at $T_C \sim 122^\circ\text{C}$ (Figure S2).

Supporting text 2:

Bulk behaviour of the symmetric PS-*b*-PLLA used in this work – SAXS

SAXS measurements were carried out using a rotating anode X-ray generator (Rigaku) equipped with a Cu target and operated at 2.4 kW. A confocal optics (Osmic) was used to irradiate the sample with a focused X-ray beam of Cu-K α (1.54 Å). The monochromatic beam was collimated using a system of three pinholes and had a diameter of ~ 350 μm at the sample position. The entire path of the X-ray beam was evacuated at $\sim 10^{-2}$ mbar. The scattered radiation was recorded on a Bruker Hi-Star multi-wire proportional chamber. Scattering patterns were acquired in the form of 1024 x 1024 pixel frames and calibrated using silver behenate. The exposure time was 1 h.

The SAXS measurements (Figure S3) show that crystallization of PLLA in bulk symmetric PS-*b*-PLLA can be suppressed by thermal quenching. Discs of bulk PS-*b*-PLLA were heated to 180°C and then quenched in liquid nitrogen or cooled to room temperature at -1 K/min. Strongly segregated symmetric bulk BCPs commonly form lamellar morphologies. However, only in the SAXS pattern of quenched PS-*b*-PLLA (Figure S3a) four reflections with length ratios of their scattering vectors q corresponding to 1:2:3:4 appear. This peak pattern suggests that an ordered lamellar domain structure with a spacing $L_0 = 37$ nm formed in the bulk melt of symmetric PS-*b*-PLLA that persisted thermal quenching. The SAXS profile of PS-*b*-PLLA cooled at -1 K/min (Figure S3b) does not show any significant features, which indicates the absence of a well-ordered nanoscopic domain structure.

Supporting text 3:

PLLA crystallinity and PLLA etching

The PLLA domains occupy only a small volume portion of the PS-*b*-PLLA/AAO nanocomposites (~5 % for $D = 180$ nm). Furthermore, only a fraction of the volume occupied by the PLLA domains will be crystalline. The PLLA crystallizes in the small separated volumes of PLLA domains located in AAO nanopores. While only a small fraction of the separated PLLA volumes contains heterogeneous nuclei, in the other separated PLLA volumes crystallization can only be initiated by homogeneous nucleation – alternatively, the PLLA does not crystallize at all. The clear indications of retarded crystallization inside the PS-*b*-PLLA nanorods apparent from the WAXS investigations (main manuscript, Figure 5) are consistent with these arguments. Finally, the PLLA domains likely contain amorphous regions at their large interfaces to the PS domains and to the AAO nanopore walls. The small volume fraction of crystalline PLLA did not allow us acquiring meaningful DSC curves of PS-*b*-PLLA confined to AAO. It should be noted that Guan et al. reported difficulties to acquire DSC traces even for PLLA homopolymer confined to AAO (Guan2015). On the other hand, release of the PS-*b*-PLLA by etching the AAO results in hydrolysis of the PLLA blocks; this makes DSC scans of released PS-*b*-PLLA nanorods impossible. Hence, we could not employ DSC as a method to study the crystallization of the PLLA in PS-*b*-PLLA confined to AAO nanopores.

Hydrolysis of crystalline PLLA is likely slower than hydrolysis of amorphous PLLA because in the former case the free energy required to remove a lactyl unit from the crystal lattice needs to be compensated – removal of lactyl units from PLLA crystals is likely associated with a higher kinetic free energy barrier than removal of a lactyl unit from amorphous PLLA. Therefore, low degrees of crystallinity, as expected for the PS-*b*-PLLA nanorods, may facilitate PLLA degradation. A second issue influencing PLLA degradation is the access to the PLLA domains. For example, sheltering of PDLLA domains by PS in randomly oriented grains of bulk PS-*b*-PDLLA was reported to hamper degradation of the PDLLA (Zalusky2001, Zalusky2002). We assume that the main obstacle for PLLA hydrolysis in PS-*b*-PLLA nanorods is encapsulation of the PLLA domains by PS. Indeed, we occasionally observed apparently solid PS-*b*-PLLA nanorod segments presumably containing intact PLLA domains that were not removed by hydrolysis. However, encapsulation of PLLA domains related to grain boundaries is naturally not an issue in the case of PS-*b*-PLLA nanorods. The larger surface area of PS-*b*-PLLA nanorods as compared to bulk PS-*b*-PLLA specimens should facilitate the access of the base to the PLLA domains. Moreover, we found large amounts of PS-*b*-PLLA nanorods broken into shorter fragments during release (Figures 2-4 of the main manuscript) so that access of bases to the PLLA domains from both fractured surfaces was possible.

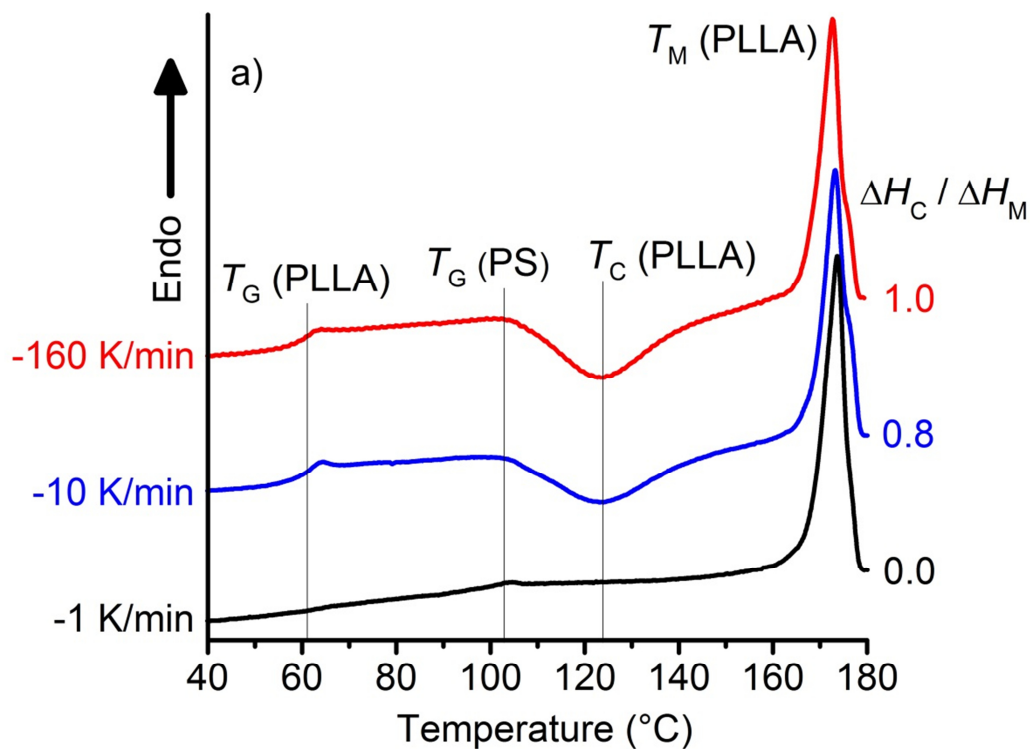


Figure S1. Differential scanning calorimetry on bulk symmetric PS-*b*-PLLA. Displayed are the second heating runs obtained after cooling at -160 K/min, -10 K/min and -1 K/min. For each heating run, the ratio $\Delta H_C / \Delta H_M$ of the enthalpy ΔH_C associated with exothermic PLLA cold crystallization and the PLLA melting enthalpy ΔH_M is given. Moreover, the glass transition temperatures $T_G(\text{PLLA})$ and $T_G(\text{PS})$ of the PLLA and PS blocks, the peak temperature of the exothermic PLLA crystallization peaks $T_C(\text{PLLA})$ as well as the peak temperature of the endothermic PLLA melting peaks $T_M(\text{PLLA})$ are indicated.

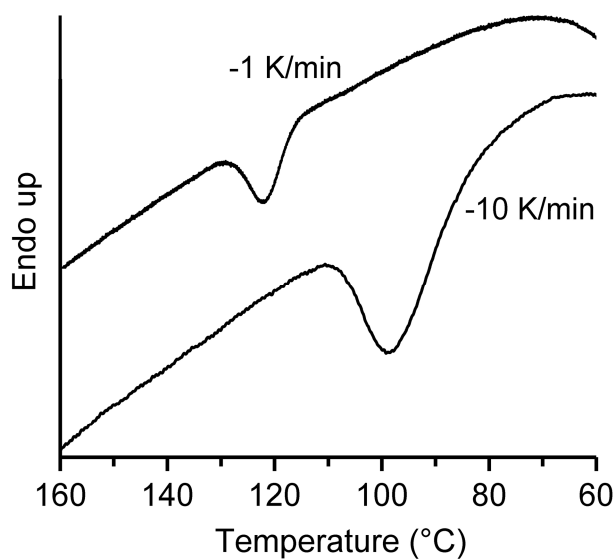


Figure S2. Differential scanning calorimetry on bulk symmetric PS-*b*-PLLA obtained with a Perkin Elmer DSC 8500. The exemplary cooling runs were taken at cooling rates of -1 K/min and -10 K/min after annealing the PS-*b*-PLLA for 10 minutes at 190°C.

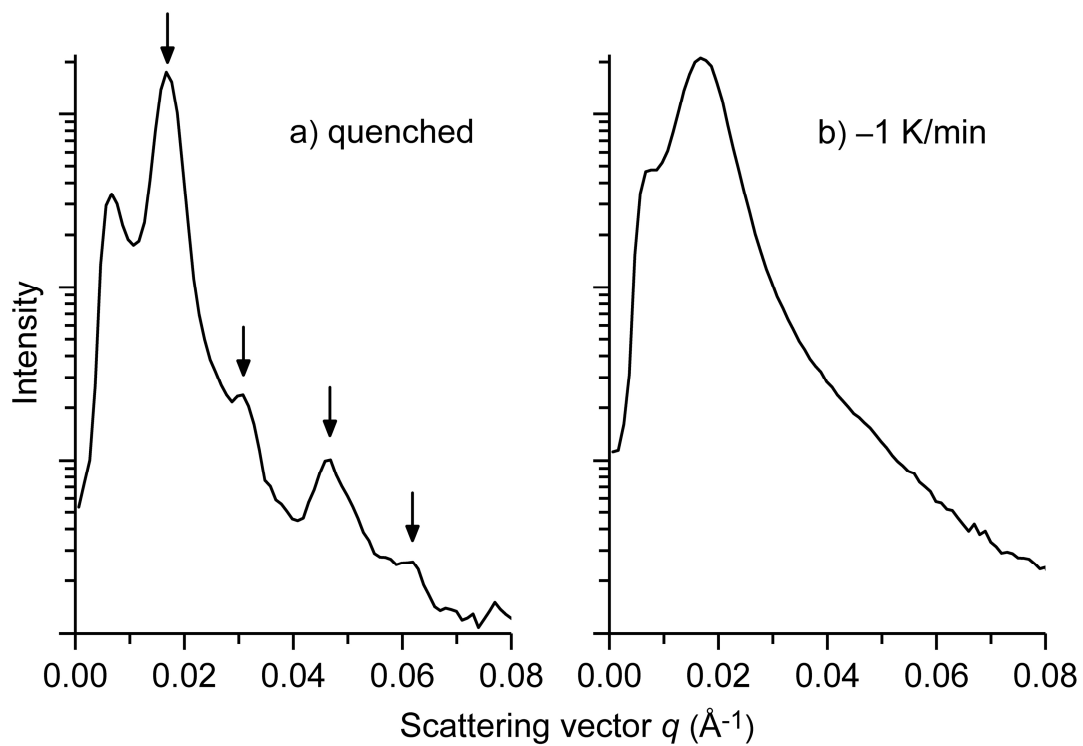
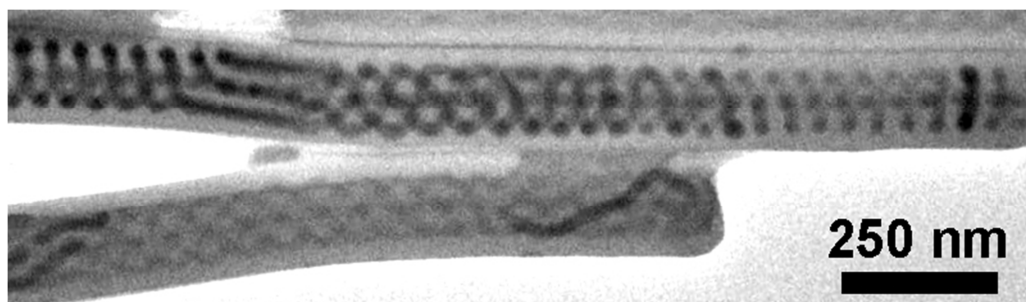
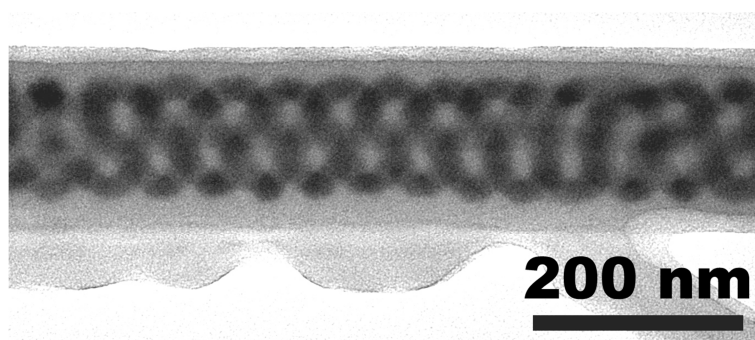


Figure S3. SAXS profiles of a) quenched bulk symmetric PS-*b*-PLLA and b) bulk symmetric PS-*b*-PLLA cooled to room temperature at -1 K/min. Higher-order peaks in panel a) are marked with arrows.



a)



b)

Figure S4. TEM images of released nanorods consisting of asymmetric polystyrene-*block*-poly(vinylpyridine) (PS-*b*-P2VP; $M_n(\text{PS}) = 50000 \text{ g/mol}$; $M_n(\text{P2VP}) = 16500 \text{ g/mol}$) prepared as described by Wang and co-authors (Wang2009). Both the PS and P2VP blocks were atactic and, therefore, non-crystallizable. After release from the AAO template, the P2VP minority domains, which are surrounded by a PS matrix, were stained with iodine and appear dark. a) Overview; b) detail of a triple P2VP helix winding about a straight central P2VP cylinder.

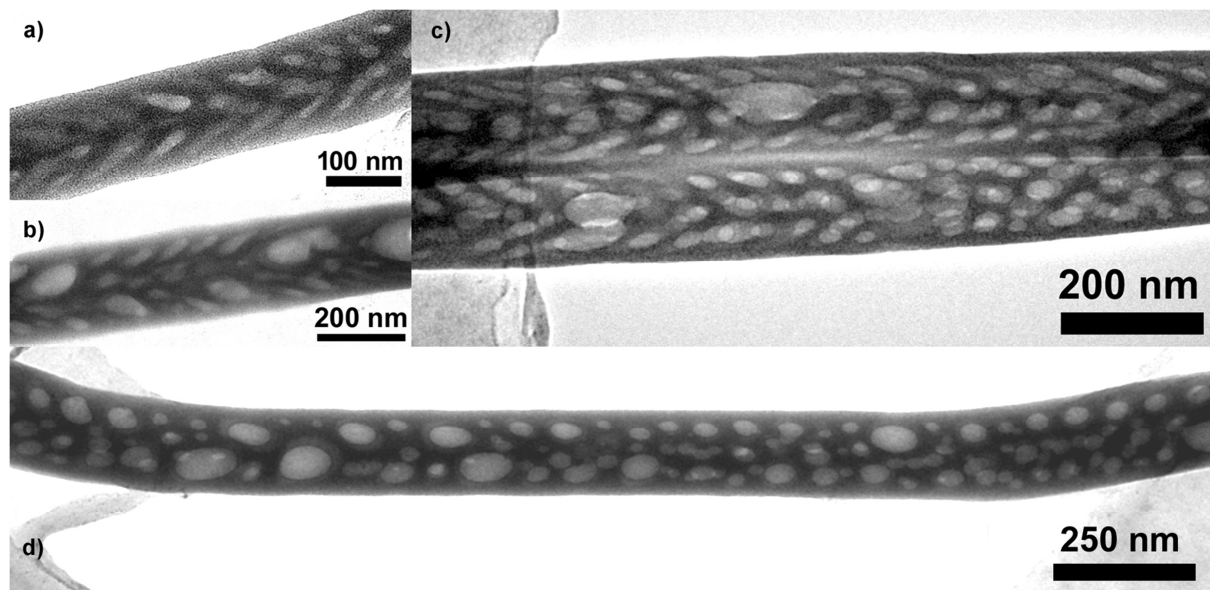


Figure S5. PS nanorods obtained with slightly asymmetric PS-*b*-PLLA (45 vol-% PLLA; M_n (PS) = 21000 g/mol; M_n (PLLA) = 19500 g/mol; M_w/M_n 1.11; obtained from Polymer Source Inc., Dorval, Canada) after isothermal crystallization at $T_C = 85^\circ\text{C}$ ($D/L_0 \sim 4.8$). The PLLA initially located at the positions of the voids was hydrolyzed. Sample preparation and crystallization was carried out exactly in the same way as in the case of the PS nanorods obtained with symmetric PS-*b*-PLLA displayed in Figure 2 of the main manuscript (see Experimental Section of the main manuscript). a), b) Side view of voids initially occupied by PLLA indicating the arrangement of PLLA crystals in fishbone-like patterns; c) voids initially occupied by PLLA with different orientations; d) top view of voids initially occupied by PLLA indicating that the PLLA crystals had an ellipsoidal contour.

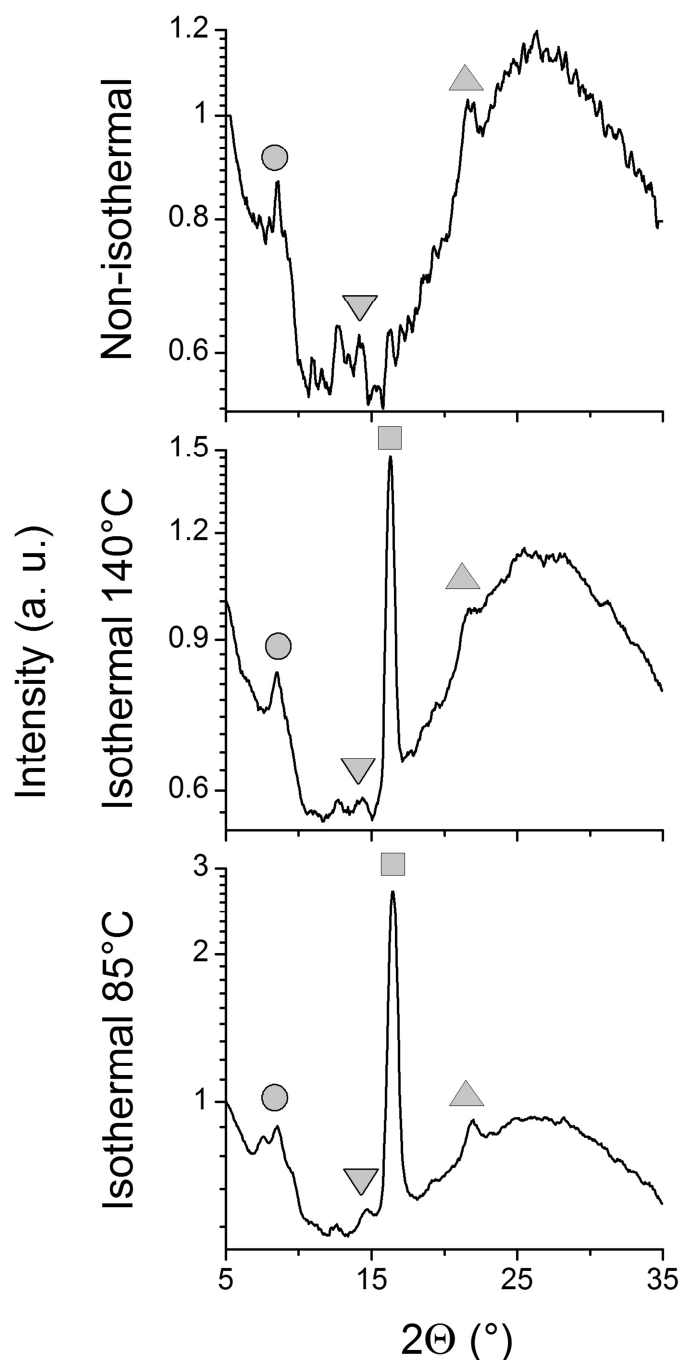


Figure S6. $\Theta/2\Theta$ scans of nanorods confined to self-ordered AAO ($D = 60$ nm; nanopore depth $60 \mu\text{m}$) consisting of slightly asymmetric PS-*b*-PLLA (45 vol-% PLLA; M_n (PS) = 21000 g/mol; M_n (PLLA) = 19500 g/mol; M_w/M_n 1.11; obtained from Polymer Source Inc., Dorval, Canada) after non-isothermal crystallization at a cooling rate of -1 K/min, isothermal crystallization at $T_C = 140^\circ\text{C}$ and isothermal crystallization at $T_C = 85^\circ\text{C}$. Sample preparation, crystallization and WAXS measurements were carried out in exactly the same way as in the case of the nanorods consisting of the symmetric PS-*b*-PLLA (see Experimental Section of the main manuscript).

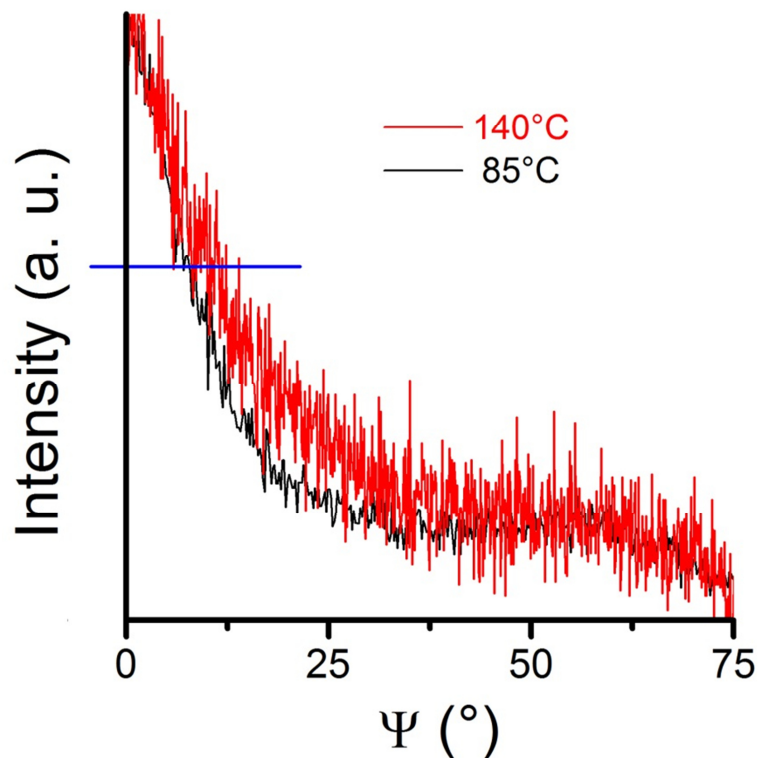


Figure S7. Normalized Schulz scans of arrays of nanorods consisting of slightly asymmetric PS-*b*-PLLA (45 vol-% PLLA; M_n (PS) = 21000 g/mol; M_n (PLLA) = 19500 g/mol; M_w/M_n 1.11; obtained from Polymer Source Inc., Dorval, Canada) located inside the aligned nanopores of self-ordered AAO ($D = 60$ nm; nanopore depth 60 μ m) for the (110)/(200) reflection of α -PLLA after isothermal crystallization at $T_C = 85^\circ\text{C}$ and isothermal crystallization at $T_C = 40^\circ\text{C}$. Sample preparation, crystallization and the measurements of the Schulz scans were carried out exactly in the same way as in the case of the nanorods consisting of the symmetric PS-*b*-PLLA (see Experimental Section of the main manuscript). The blue line indicates the half height of the maximum at $\psi = 0^\circ$.

Guan2015: Guan, Y.; Liu, G.; Ding, G.; Yang, T.; Mueller, A. J.; Wang, D. Enhanced Crystallization from the Glassy State of Poly(L-lactic acid) Confined in Anodic Alumina Oxide Nanopores. *Macromolecules* **2015**, *48*, 2526-2533.

Wang2009: Wang, Y.; Qin, Y.; Berger, A.; Yau, E.; He, C.; Zhang, L.; Gösele, U.; Knez, M.; Steinhart, M. Nanoscopic Morphologies in Block Copolymer Nanorods as Templates for Atomic-Layer Deposition of Semiconductors. *Adv. Mater.* **2009**, *21*, 2763–2766.

Zalusky2001: Zalusky, A.; Olayo-Valles, R.; Taylor, C.; Hillmyer, M. Mesoporous polystyrene monoliths. *J. Am. Chem. Soc.* **2001**, *123*, 1519-1520.

Zalusky2002: Zalusky, A.; Olayo-Valles, R.; Wolf, J.; Hillmyer, M. Ordered nanoporous polymers from polystyrene-poly lactide block copolymers. *J. Am. Chem. Soc.* **2002**, *124*, 12761-12773.